Evolution in Polymer Technology Journal

Research Article *Volume 3 Issue 1*

Fabrication, Characterization and Biocompatible Properties of β-Chitin/Silk Fibroin/MCM-41 Composite Scaffolds for Bone Tissue Engineering Applications

Mohammad Azadi[1]*, Abbas Teimouri[1], Reihaneh Taherifard[1], Zahra Shams Ghahfarokhi[2], Jamshid karvani Aliabadi[3] and Nafiseh Mobadi[1]

[1]Department of Chemistry, Payame Noor University, Iran

[2]Department of Chemistry, Faculty of Science, University of Birjand, Birjand, Iran

[3]Faculty of Science, Shahrekord University, Rahbar Blvd, Shahrekord, Iran

***Corresponding author:** Dr. Mohammad Azadi, Department of Chemistry, Payame Noor University (PNU), Isfahan, P.O. Box 81395-671, Iran, Tel: +98 31 33521804; Fax: +98 31 33521802; Email: mohammad_azadi60@yahoo.com

Received Date: January 19, 2020; **Published Date:** February 14, 2020

Abstract

β -chitin/silk fibroin/MCM-41 (CT/SF/MCM-41) composite scaffolds were synthesized using the freeze-drying method by blending CT hydrogel, SF and MCM-41 in different organic/inorganic weight ratios. The prepared MCM- 41 and composite scaffolds were characterized using the scanning electron microscope (SEM), fourier transform infrared spectroscopy (FT-IR), X-ray diffraction (XRD), and thermo gravimetric analysis (TGA) studies. The composite scaffolds were found to have 76-81% porosity with a well-defined interconnected porous construction. Moreover, the cell viability, attachment and proliferation were investigated using 3-4, 5-dimethylthiazol-2yl {-2, 5- diphenyl-2H-tetrazoliumbromide} (MTT), Dulbecco's modified eagle medium (DMEM) solution; the mouse preosteoblast cell proved the cytocompatible nature of the composite scaffolds with well-improved proliferation and cell attachment. These results implied that these materials could be a candidate for bone tissue engineering applications.

Keywords: β-chitin; Silk fibroin; MCM-41; Composite scaffold; Tissue engineering

Abbreviations: SF: Silk Fibroin; CT: Chitin; TEOS: Tetraethyl Orthosilicate; CTAB: Cetyltrimethylammonium Bromide; DMSO: Dimethyl Sulfoxide; DMEM: Dulbecco's Modified Eagle Medium; FBS: Fetal Bovine Serum.

Introduction

Tissue engineering employs three-dimensional (3-D) porous composite scaffolds with an appropriate pore size and high porosity for mechanical stability to regenerate or repair the damaged tissue in order to support cell attachment and expansion, well as degrading at a rate comparable that of the new tissue growth. In other words a scaffold must mimic the natural extracellular environment of the tissue, certain mechanical strength, the time-space matching characteristic of the degradation disappearance of materials, and the new tissues structure [1-3]. A full understanding of the compositions, structures, and biomechanical and biochemical properties of the natural bone for designing the ideal biomimetic artificial scaffold is required. Natural bone is a complex organic-inorganic Nano-composite material with different part materials, including about 10-20%

collagen, 60-70% Nano hydroxyapatite (nHAp), and 9-20% water, by weight [4,5].

Silk fibroin (SF) is a biomaterial with impressive oxygen penetrability, mechanical properties, biocompatibility and biodegradability. So, SF has been used for the tissue engineering [6]. The problems with the nHAp ceramic, such as intrinsic fragileness, migration of nHAp particles from the implanted sites and poor formability, can be tacked by the adhesion of the nHAp ceramic with biopolymers such as SF and chitin (CT). The addition of SF increases the rigidity of the nHAp ceramic. However, the nHAp/SF composite cannot meet the requirement for bone replacement due to its inadequate formability and flexibility [7-10].

CT is one of the most plentiful, readily available and less expensive organic materials in nature. It is known to be one of hetero-polysaccharides with biodegradability, biocompatibility, non- toxicity, mineralization (calcification), wound healing, and antibacterial and anti-inflammatory properties. CT can be easily processed into gels, membranes, nanofibres, beads, nanoparticles, scaffolds and sponges. CT and its derivatives have been used for a variety of applications such as water treatment, textiles, paper, agriculture, cosmetics, food and health supplements, and wound dressings. Also, they can be used in the scaffolds for tissue regeneration and osteogenesis. Therefore, they can be employed as bone substitutes for bone repair and reconstruction. The degradation product is D-glucosamine, which further enhances the deposition of collagen in the presence of a wound [11-24].

MCM-41 is a mesoporous silicate molecular sieve formed from closely packed silica-coated micelles of a surfactant template. Mesoporous materials are characterized as having high surface area, and tunable and accessible pores. Due to their textural properties of surface porosity, the ordered mesoporous materials have shown to be excellent candidates for two biomedical applications: local drug delivery systems and bone tissue regeneration. These materials are able to bond to the living bone when implanted through the formation of a nonstoichiometric carbonated hydroxyapatite (CHAp) of nanometrical size. This bioactive bond ensures the implant osteo- integration, and its degradation products promote the bone tissue regeneration. Moreover, these materials can be loaded with osteogenic agents promoting the new bone formation in vivo and can also be applied as scaffolds for bone tissue engineering.[15-24] Studies have exhibited that the composite scaffolds of CT/SF and nHAp/MCM-41 can improve the cell viability and the biodegradation, but their formability and mechanical strength are not good [25-29].

However, the influence of MCM-41 on the SF/CT composite scaffolds is not well understood. Following our recent study on the structure of composite scaffolds [30-38], in this work we focused on the fabrication, characterization, biomineralization, porosity, water-uptake capacity, biodegradation, bioactivity, and mechanical and in vitro properties of the nanocomposite scaffolds CT/SF/MCM-41 for bone tissue engineering applications.

Experimental Section

Materials

CT (degree of acetylation 72.4%) was purchased from Koyo Chemical Co., Ltd., Japan. LiBr, sodium acetate, ethanol, methanol, glutaraldehyde, n-hexane, ammonium hydroxide, sodium carbonate, tetraethyl orthosilicate (TEOS), cetyltrimethylammonium bromide (CTAB), dimethyl sulfoxide (DMSO), CaCl2.2H2O and all other solvents and chemicals were bought from Sigma- Aldrich. Raw cocoons of silkworm, Bombyx mori, were supplied from Sericulture Farm, Natanz, Iran. Cellulose dialysis cassettes (Slide-A-lyzer, MWCO 12000 Da (Sigma)) were used to remove the solvent impurities from the SF solution. For the in vitro study of cytotoxicity, a mouse preosteoblast cell line (MC3T3-E1) was purveyed by Riken Cell Bank (Ibaraki, Japan). Dulbecco's modified eagle medium (DMEM), ascorbic acid and 3-4, 5-dimethylthiazol-2yl {-2, 5-diphenyl-2H-tetrazoliumbromide} (MTT) were purchased from Sigma-Aldrich, USA. Fetal bovine serum (FBS) was purchased from Wisent (Montreal, Canada). Hen lysozyme was purchased from Cell Bank, Pasteur Institute of Tehran.

Preparation of calcium solvent

The calcium solvent was prepared as described in the literature [39]. To make clear calcium solvent, we dispersed 850 g $CaCl_2.2H_2O$ in 1 liter of methanol and refluxed it for 30 minutes; was kept overnight at room temperature and after that, filtration was done.

Preparation of CT hydrogel

5g of CT was added to 1 liter of calcium solvent and stirred forcefully for 2 days at room temperature. The solution was filtered to remove the un-dissolved traces and get a clear CT solution. Excess water was added to this solution to break the bond between CT and $CaCl_2$ and stirred for 2 h powerfully. After standing overnight, it was filtered and dialyzed against distilled water for 48 h to obtain the pure CT hydrogel [12].

Preparation of regenerated SF

Bombyx mori silk cocoons were cut into fourths. Then, sericin was removed by boiling the cocoons in a 0.02 M Na2CO3 solution for 45 minutes. The fibroin extract was then washed deeply with distilled water, dissolved in the 9.3 M LiBr solution at room-temperature, and warmed at 60°C for 4 hours. The solution was dialyzed with ultrapure water

for 2 days to remove the residual LiBr and then centrifuged. Gravimetric analysis showed that the concentration of the derived aqueous silk solution was about 2.5 wt/vol. % [6,40].

Preparation of MCM-41

MCM-41 was prepared according to the literature by dissolving the surfactant in a mixture of water/ethanol; and the ammonia solution and sodium acetate were added to this solution. After about 15 minutes stirring, a clear solution was obtained. Then, the TEOS was added at one time to this solution. The final molar composition of the resulting gel was TEOS: 1; CTAB: 0.22; sodium acetate: 0.034; NH3: 11; ethanol: 1; water: 155. After 3 h stirring at room temperature, the obtained gel was transformed to a Teflon-lined stainless-steel vessel and aged at 70°C for 5 h. The white precipitate was filtered and washed with water and then calcined in air at the heating rate of 1°C/min up to 550°C; it was maintained for 5 h before cooling down to room temperature (scheme 1) [15].

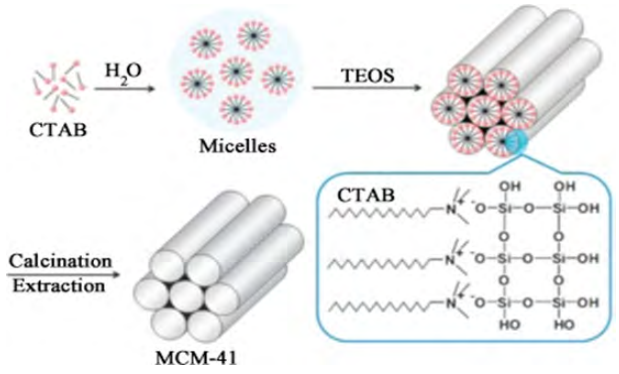

Scheme 1: The formation mechanism of MCM-41.

Preparation of Composite Scaffold

CT hydrogel was added into the silk solution and stirred for 12 h at 4°C. Then, MCM-41 was added to the solution and stirred for 24 h to disperse MCM-41 in the silk solution. The resultant solution was suspended in an ultrasonic sonicator bath to further disperse the particles and reduce the particle size. Subsequently, 0.25% (v/v) glutaraldehyde was added in the 1:32 ratio (2 h) for crosslinking. The final solution was transferred to the 24-well culture plates and pre-frozen at -20°C for 12 h. This was followed by freeze-drying (Dena vacuum industry) at -80°C for 48 h. The SF content of each specimen was scaled according to the CT/SF/MCM-41 weight ratios of 90/05/05, 80/10/10, and 70/15/15.

Characterization

The samples were characterized by X-ray diffraction (XRD, Bruker D8ADVANCE, Cu Ka radiation), the fourier transform infrared spectroscopy (FT-IR, Nicolet 400D in KBr matrix, with the range of 4000-400 cm^{-1}) and the scanning electron microscope (SEM, Philips, XI30, SE detector). To investigate the weight loss of the CT/SF/MCM-41 composite scaffolds during thermo gravimetric analysis (TGA), a test was carried out using a DuPont TGA 951 at temperatures ranging from room temperature to 450°C in air and at the heating rate of 10°C/min.

Porosity studies

The porosity of the scaffolds was evaluated using a liquid displacement approach.1 Hexane served as the displacement liquid because it was a non-solvent agent for silk and could be easily permeated through the scaffold without any shrinkage or swelling of the scaffold. Scaffolds were cut into 1 cm×1 cm×1 cm pieces and immersed in a cylinder containing a clarified volume of hexane (V1). The volume of hexane and the hexane-saturated scaffold was noted as V2 and achieved after the scaffold was placed in hexane for 1 h. The volume difference (V2 _ V1) was the volume of the composite scaffold. The residual hexane volume in the graduated cylinder after the removal of the scaffold was recorded as V3. The quantity (V1_V3), the volume of hexane within the scaffold, was defined as the void volume of the scaffold. The total volume of the scaffold was V = (V2_V1) + (V1_V3) = V2_V3. The porosity of the scaffold (ε) was measured as follows: ε (%) = (V1_V3)/(V2_V3) × 100.

Water-uptake capacity

The scaffolds were immersed in water at room temperature for 48 h in order to ensure water saturation into the open pores. The water uptake of the porous samples was calculated as Water- uptake (%) = (Ww _ Wd)/Wd × 100, where Ww and Wd represent the wet weight of the sponges and the initial dry weight scaffolds, respectively.

Mechanical properties

Compressive strength and modulus of the composite scaffolds were measured in the dry state at a crosshead speed of 2 mm/min in a material prufung 1446-60 machine (Zwick). The samples with a size of 1 cm×1 cm×1 cm were used in the compressive property test. In vitro degradation

The degradation of the SF and CT/SF/MCM-41 composite scaffolds was examined in a phosphate buffered saline (PBS) medium containing lysozyme (10,000 U/ml) at 37°C for different time intervals (1, 4, 7, 14, 21 and 28 days). Wo and Wt represent the initial weight and the dry weight of scaffolds, respectively. After a specified period, the scaffolds were washed in deionized water for the removal of the surface adsorbed ions and lyophilized. The degradation of the scaffolds was assayed using the following formula:

$$\text{Degradation\%} = (Wo - Wt)/Wo \times 100$$

Degradation rate was recorded as mean ± S.D. (n = 5).

In vitro biomineralization

Composite scaffolds with equal weights and shapes were placed in the simulated body fluid (SBF) solution and then incubated at 37 °C in closed Falcon tubes for various time intervals (1, 4, 7 and 14 days). The SBF solution was prepared as described in the literature [41]. After each period, the scaffolds were washed three times with deionized water for the removal of the adsorbed minerals. After 7 and 14 days, the scaffolds were freeze dried and characterized using SEM and FT-IR for mineralization.

In vitro evaluation of cytotoxicity

The MTT test was used as a sign of the relative cell viability [42]. Mouse preosteoblast cell line MC3T3-E1 was employed to estimate the in vitro cytotoxicity of the extractions. The passaged (cells less than passage 7) and isolated cells were trypsinised, pilled and suspended in a known amount of the DMEM media. The cell concentration of 1×10^5 cells/ml^{-1} was transferred onto the 24-well tissue culture plates overnight. The samples were sterilized by placement in ethanol; this was followed by UV irradiation for 30 minutes. The scaffolds (1cm × 1cm × 1cm) were immersed in separate sterile tubes with the 5 ml DMEM solution and incubated at 37°C for 24 h. To examine the in vitro cytotoxicity of the extractions, a 4 ml extraction of each sample was collected. The culture media were changed with the extraction every 2 days. MTT assay was managed in 1, 3 and 7days by changing the media with the MTT solution in the wells for 4 h. The MTT solution was removed and formazan crystals were dissolved in DMSO. A micro plate reader (Bio-RAD 680, USA) recorded the optical density in a spectrophotometer at the stimulus wavelength of 540 nm. DMSO served as a blank. The same numbers of cells in contact with the culture media were taken as the control groups. Statistical analysis

Statistical analysis was performed using SPSS v.16.0 software. Data were expressed as the mean ± Significant if ρ values obtained from the test were less than 0.05. ($\rho < 0.05$).

Results and Discussions

SEM Analysis

Figure 1 illustrates the SEM micrographs of the samples. In the pure CT (Figure 1a), the number of the interconnected pores was high. The pure SF scaffold showed a macroporous construct with interconnected open pores and a size ranging from 100 to 200 µm (Figure 1b). The calcined MCM- 41 particles had a distorted sphere shape. The particle size ranged from 250 to 400 nm. However, some larger particles of about 1000 nm could be seen in the SEM image (Figure 1c). In the scaffolds, open interconnected pores could enhance fluid exchange and native tissue ingrowth. (Figure 1d-f). The MCM-41 particles made the pore walls rough. These were beneficial for cell adhesion. In the composite scaffolds, the amount of MCM-41 managed the average porosity and the degree of interconnectivity. As it is obvious from Figure 1 (d-f), the increase in the amount of MCM-41 caused the decrease in the number of pores.

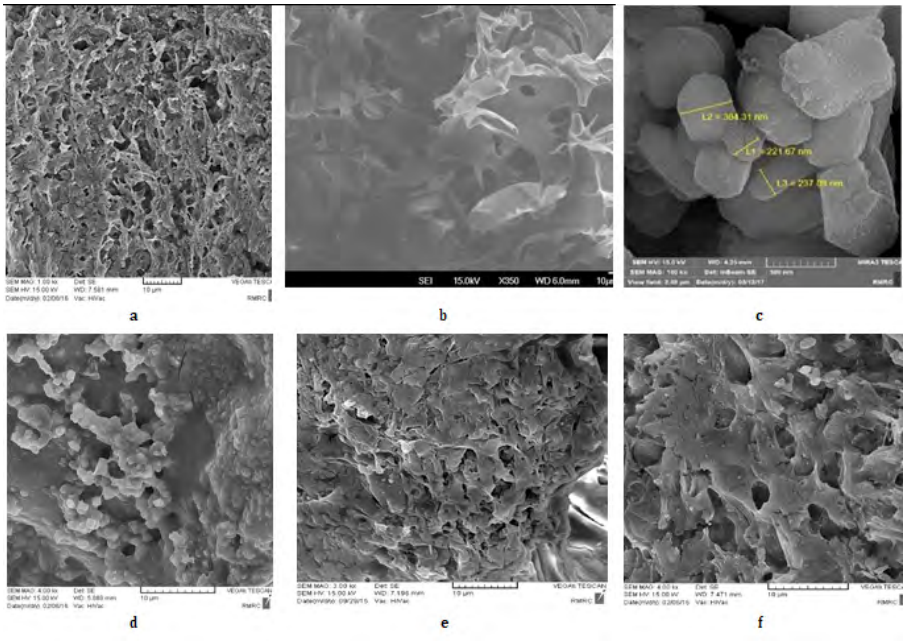

Figure 1: SEM images of (a) pure CT, (b) pure SF, (c) pure MCM-41, d) Composite 90/05/05, (e) composite 80/10/10, and (f) composite 70/15/15.

FT-IR studies

As a characterization tool, FT-IR can provide certain structural clues regarding the overall molecular structure of the unknown substance. It is a simple and reliable technique widely used in both organic and inorganic chemistry. Figure 2A illustrates the FT-IR spectra of the samples in the spectral range of 4000-400 cm^{-1}. The FT-IR spectrum of CT showed peaks at 3430 cm^{-1} (O-H stretching vibration), 1601 cm^{-1} (amide I), and 1392 cm^{-1} (C-H bending) (Figure 2a). The peaks at 1625 ± 5 cm^{-1} (amide I), 1525 ± 5 cm^{-1} (amide II), and 1265 ± 5 cm^{-1} (amide III) were attributed to the silk II structural conformation (β-sheet). The absorption bands at 1520 cm^{-1} (amide II) and 1226 cm^{-1} (amide III) were related to the silk I structural form (random coil and α-helix) (Figure 2b) [12]. FT-IR spectrum of MCM-41 showed peaks at 1090 and 1223 cm^{-1} (T–O asymmetric stretching, internal and external, respectively) and 800 cm^{-1} (T–O symmetric stretching) due to TO4 vibrations (T = Si), which could be assigned to the bending Si–O–Si, and a band at 454 cm^{-1} due to the bending of T-O. The band at 1630 cm^{-1} could be ascribed to the Si–O stretching overtone also appeared clean with the evacuation of the hosts at 400°C [29].

The absorption bands at 1550 and 1239 cm^{-1} could be characteristic of the amide II and the amide III of SF in the CT/SF/MCM-41 composite scaffolds. The OH absorption of SF in CT/SF/MCM-41 composite scaffolds could be observed at 3284-3430 cm^{-1}, which became wider than SF itself. So, the characteristic absorptions of OH in CT/SF/MCM-41 composite scaffolds suggested the formation of the hydrogen bond between MCM-41, SF and CT. The hydrogen bonds may also exist between -NH2 and MCM-41 (Scheme 2). From spectrum (d-f), it was found that the incorporation of MCM-41 into CT hydrogel caused the broadening of the peak at 3430 cm^{-1} (characteristic of CT); this was due to the intermolecular hydrogen bonding between –NH2 group of CT and –OH group of MCM-41. The characteristic peaks of MCM-41 were present in the spectrum of the composite scaffolds. The intensity of the peaks at 470 and 543 cm^{-1} was less that in (d) scaffold, because the concentration of MCM-41 was less. But in the (d) scaffold the peaks were resolved and intensity was also increased. MCM-41 and SF organically cross-linked together to form a structure similar to the natural bone (Scheme 2).

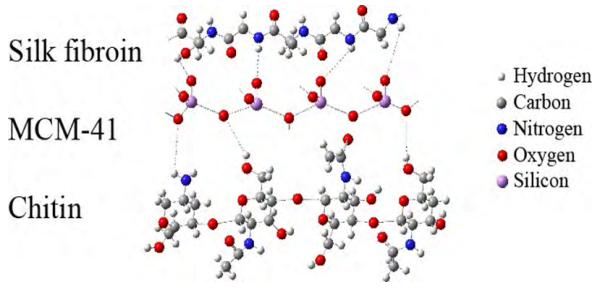

Scheme 2: The interactions between the CT, SF and MCM-41 in composite scaffolds.

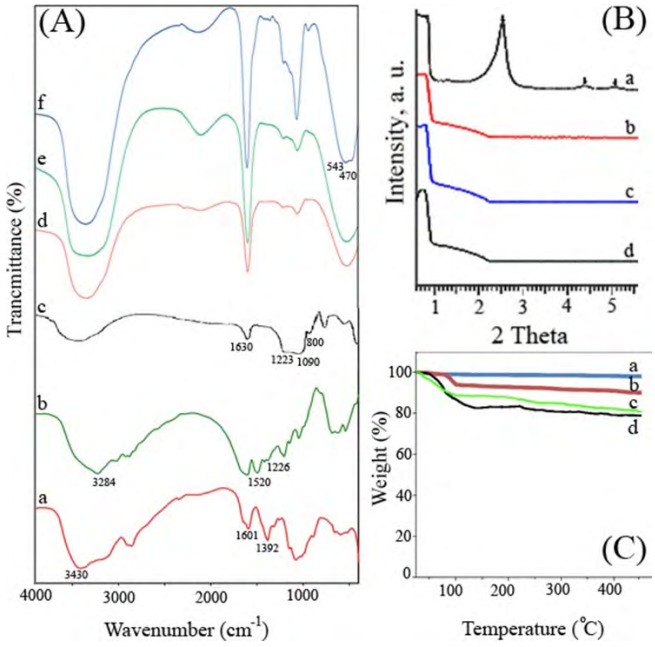

Figure 2: A) FT-IR spectra of (a) pure CT, (b) pure SF, (c) pure MCM-41, (d) composite 90/05/05, (e) composite 80/10/10, and (f) composite 70/15/15, B) XRD patterns of (a) pure MCM-41, (b) composite 90/05/05, (c) composite 80/10/10, and (d) composite 70/15/15 and C) TGA curves of (a) pure MCM-41, (b) composite 70/15/15, (c) composite 80/10/10, and (d) composite 90/05/05.

XRD Analysis

XRD has led to a better understanding of chemical bonds and non-covalent interactions. Figure 2B (a-d) shows the XRD patterns for the pure MCM-41 and composite scaffolds with the weight ratios of MCM-41. The sample MCM-41 exhibited three distinct diffraction peaks that could be indexed as (100), (110) and (200) in the hexagonal symmetry revealing the high structural organization of the mesoporous structure [15,29]. In the composite scaffolds, these peaks had no intensity in comparison to the pure MCM-41. This could be due to the interactions between the CT, SF and MCM-41 in the composite scaffolds mentioned in the FT-IR section (Scheme 2).

TGA Analysis

The thermal stability and the compositional fraction of the composite scaffolds were evaluated by TGA. TGA curves of the pure MCM-41 and the CT/SF/MCM-41 composite scaffold are displayed in Figure 2C. TG curve of the pure MCM-41 particles showed a continuous weight loss of 8%, which could be related to water evaporation. There was no weight loss above 350°C, proposing that the pure MCM-41 was thermally stable at high temperature. The weight of three composite scaffolds decreased quickly with increasing the temperature. The initial weight loss occurred around 100°C that could be assigned to water evaporation. The thermal decomposition of the organic component in the CT/SF/MCM-41 composite scaffolds occurred mostly in the range of 200-250°C. The organic components were decomposed completely at 400°C. Since the inorganic phase of the 90/05/05 composite scaffold was less than that of others, its thermal stability was less than the others. The organic/inorganic weight ratio in the CT/SF/MCM-41 composite scaffold (Figure 2C(b)), except from water content, was computed to be 28.8/71.2, unlike the theoretical weight ratio (30/70). Thermal analysis exhibited that SF and CT molecules had well interacted with MCM-41 [3,20,21].

Porosity measurements

Pores are necessary for bone tissue growth because they allow migration, expansion and proliferation of osteoblasts cells while maintaining transport. Moreover, a porous surface increases mechanical interlocking between the natural bone and the implant biomaterial, providing better mechanical stability at this interface [43]. The porosities of the fabricated scaffolds are shown in Figure 3. When the amount of CT, which had a macroporous construct with many interconnected open pores, was increased from 70 to 90 wt%, the porosities were increased from about 76% to 81%. It would be adequate to provide a chance for the nutrient transport interconnection and cell migration [35]. The crash of the thicker pore walls with the expected agglomeration of MCM-41 particles along with the increase in the MCM-41 content (the decrease in the CT content) inside them caused the reduction in porosities. Also, as mentioned in the FT-IR section, the presence of MCM-41 in the scaffold, which held the polymer chains of CT and SF and created the interaction between them (scheme 2), caused the reduction in porosities [25,28,35]. Pore sizes were affected by the time for the growth of ice crystals.

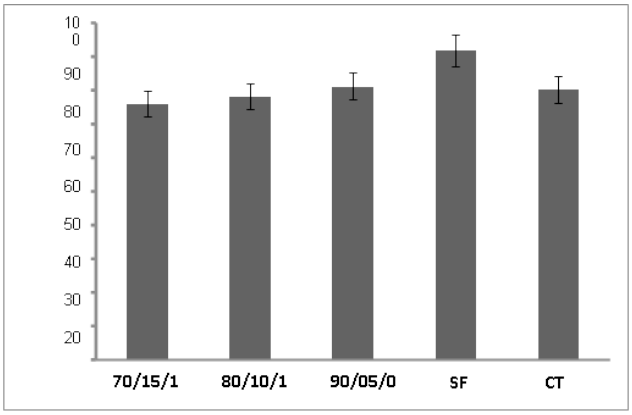

Figure 3: Porosity values of CT, SF and composite scaffolds. Data are presented as the mean ±SD (n=5). Significant difference ($p \leq 0.05$).

Water-uptake capacity

Water-uptake studies of SF, CT and CT/SF/MCM-41 composite scaffolds showed the high water- uptake capacity (Figure 4).

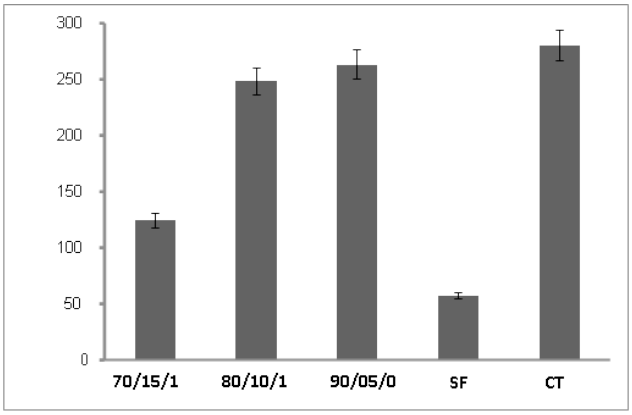

Figure 4: Water-uptake values of CT, SF and composite scaffolds. Data are presented as the mean ±SD (n=5). Significant difference ($p \leq 0.05$).

The addition of CT values from 70 to 90 wt.% increased the water- uptake of CT/SF/MCM-41 composite scaffolds. Water-uptake promoted the cells penetration into the scaffolds in a 3-Ddesign, during cell culture. In addition, water-uptake increased the pore size and the total porosity of the scaffolds. Composite scaffolds showing the higher water-uptake capacity could have a larger surface area/ volume ratio. This would make the maximum chance of cell permeation into the scaffold. So cell growth was enhanced by adhesion to the scaffold surfaces. The increase in water-uptake also allowed the samples to get nutrients from the culture media more considerably. However, while the water-uptake of scaffolds would improve cell attachment, it could also lower its mechanical properties.

Mechanical Properties

Natural bone has good mechanical properties, such as high resistance to tensile and compressive forces, low stiffness, appreciable flexibility and high fracture toughness [3]. Appropriate mechanical properties are essential to offer the correct stress environment for the neo-tissue; the mechanical strength of the scaffold should be enough to provide mechanical stability to withstand the stress before the synthesis of the extracellular matrix by the cells. Mechanical cues of cell microenvironment play a significant role in regulating cell behaviors such as migration, cell spreading, differentiation and proliferation. The compressive strength was increased inversely with the pore size, which could be described by a decrease in strut strength with increasing the pore size [22]. In this work, the influence of the MCM-41 incorporation on the compressive strength (Figure 5A) and compressive modulus (Figure 5B) of the composite scaffolds was evaluated. The addition of MCM-41 increased the pore wall thickness and the reduced pore sizes could be responsible for the high mechanical properties in the composite scaffolds, in comparison to the SF and CT.

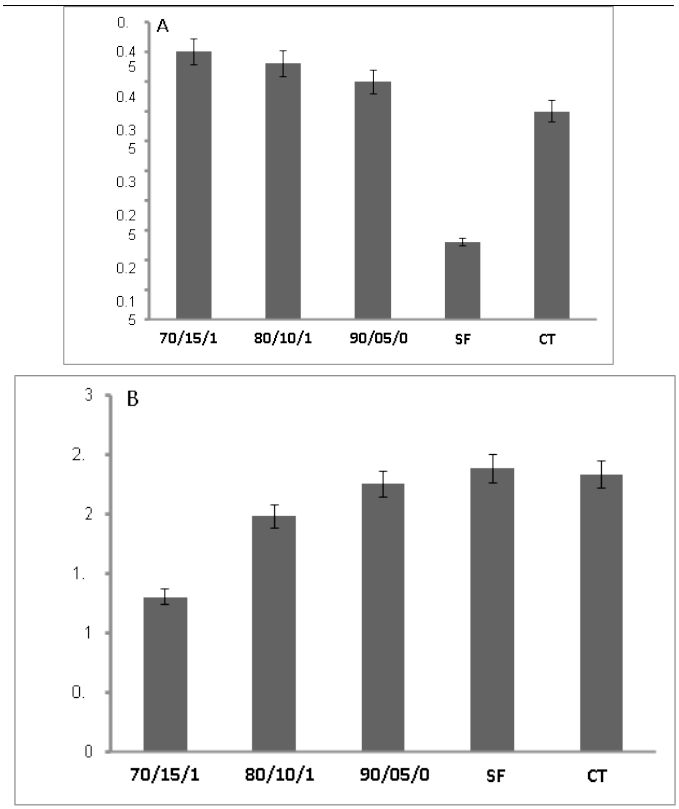

Figure 5: Mechanical properties of CT, SF and composite scaffolds with various weight percentages of SF: (A) compressive strength; (B) compressive modulus. Data are presented as the mean ±SD (n=5). Significant difference ($p \leq 0.05$).

In Vitro Degradation Studies

Figure 6 illustrates the degradation profiles of composite scaffolds after incubation in the PBS solution at 37 °C and pH = 7.4 for 4 weeks. The macromolecules of the scaffolds surface tolerated significant hydrolytic scission into small molecules (oligomeric units) which could be dissolved in PBS [19]. The percentages of the weight loss of all composites were less than 20% after 28 days. The degradation rate of the pure SF

and CT was higher than that of the composite scaffolds. The scaffolds degradation rate was decreased with the addition of the MCM-41 content (the decrease in the CT content) into the composite. The hydrophilic macromolecular chains of the CT polymer were hydrolyzed in the presence of water [13]. CT could be degraded by using lysozyme present in the human body. The samples were degraded more in the lysozyme solution with a high concentration of CT. The degradation products could further help to get more cells to the scaffold. So it promoted the bioactivity of the scaffolds [20]. These exhibited that the degradation of the composite scaffolds could be made by changing the MCM-41 or CT concentration.

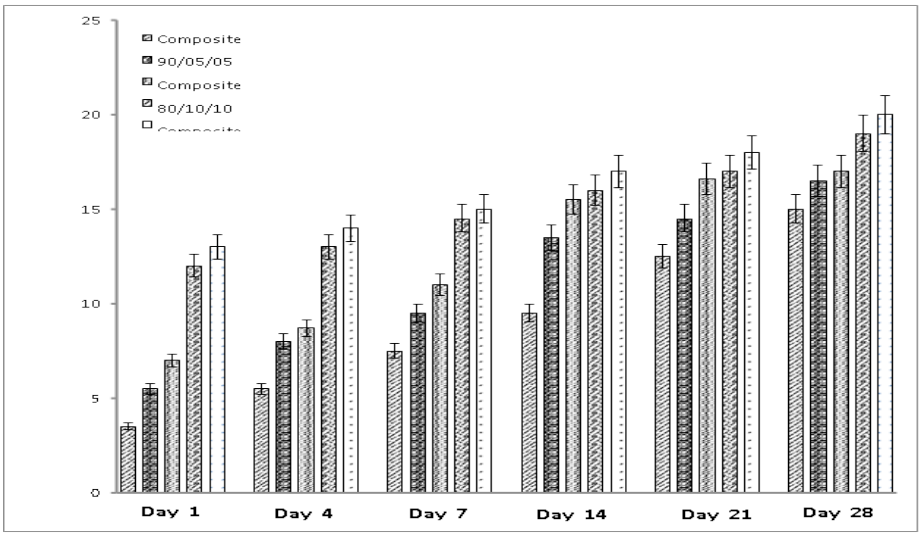

Figure 6: Degradation behavior vs time curve of scaffolds in PBS containing lysozyme at 37 ºC. Data are presented as the mean ±SD (n=5). Significant difference ($p \leq 0.05$).

In-Vitro Biomineralization Studies

The scaffolds presented a good potential to undergo mineralization at the physiological pH and temperature in the SBF solution. The apatite deposition morphology became different after 7 and 14 days of incubation. After these periods of incubation in 1× SBF, the minerals were observed to deposit on the surface of pores (Figure 7).

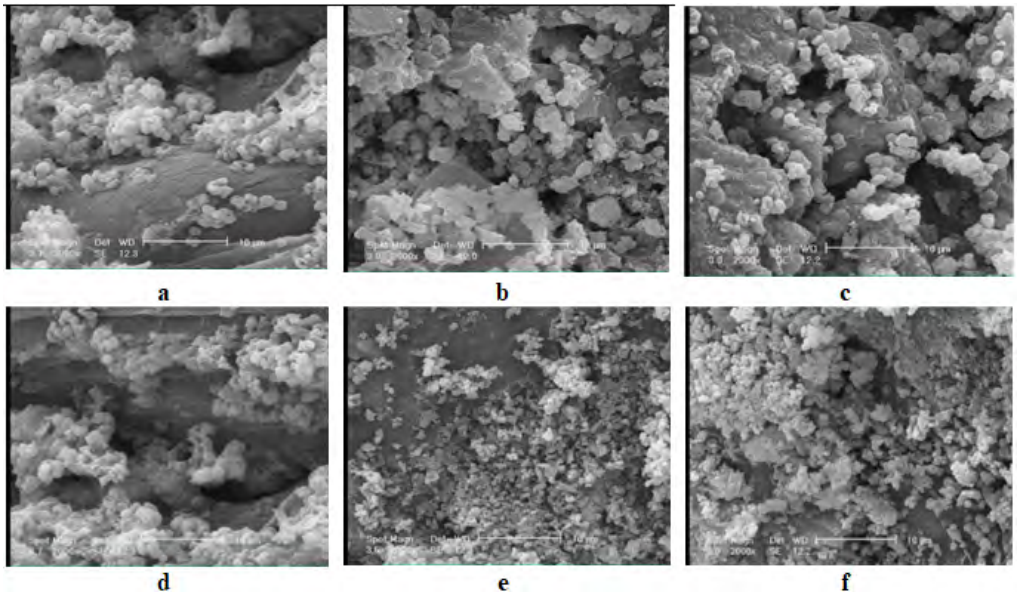

Figure 7: SEM images of (a) composite 70/15/15, (b) composite 80/10/10, and (c) composite 90/05/05 when immersed in SBF solution after 7 days and B) SEM images of (a) composite 70/15/15, (b) composite 80/10/10, and (c) composite 90/05/05 when immersed in SBF solution after 14 days. The scale bars are 10 μm in SEM images.

The FT-IR spectra displayed in Figure 8A and B showed bands at 1037 cm^{-1} and 1135 cm^{-1} were the characteristic bands of phosphate stretching vibration, while the bands at 629 and 597 cm^{-1} were due to the phosphate bending vibration. Apatite could be created more impressively in the composite when immersed in the SBF solution after 14 days. This showed that the mineral deposition was enhanced. There were many MCM-41 particles on the composite scaffolds which served as nucleation sites that decreased the surface energy minerals. So, apatite could be formed more effectively on the 70/15/15 composite. It has been implied that the formation of apatite on the scaffolds is caused by the negative charge functional groups which can further induce apatite by the formation of the amorphous calcium phosphate. The apatite nuclei were formed, and they were grown naturally by using the phosphate and calcium ions present in the medium [43].

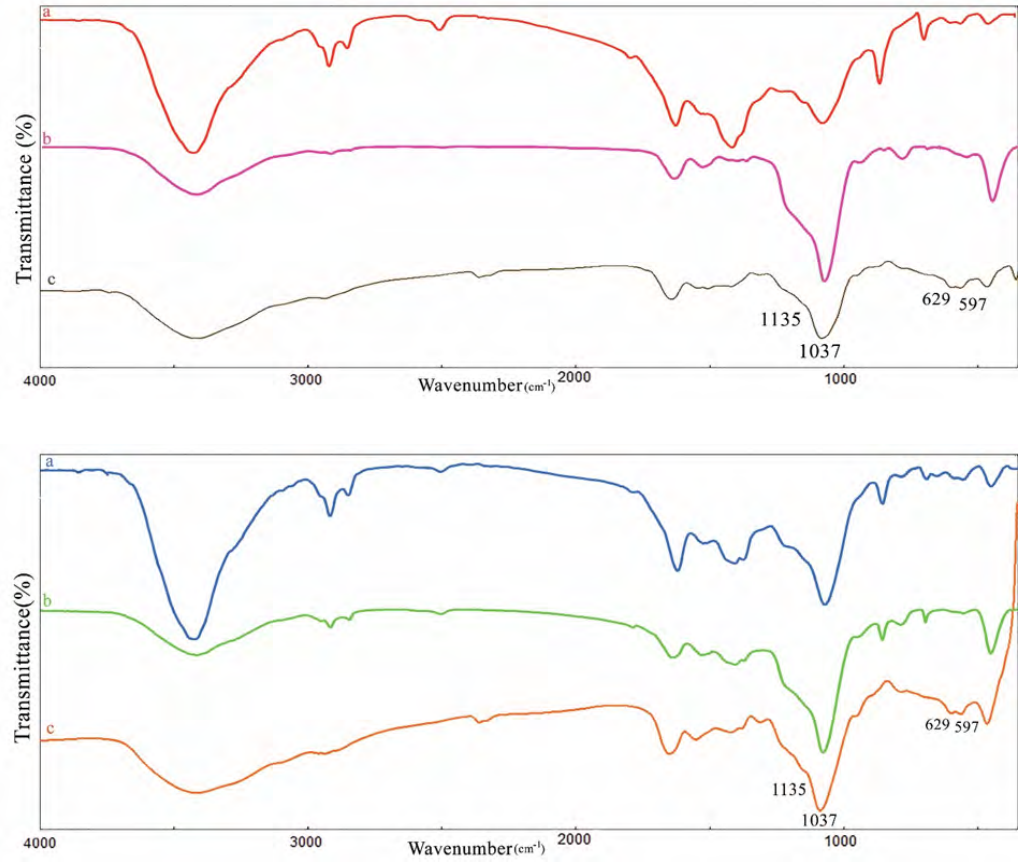

Figure 8: A). FT-IR spectrum of (a) composite 70/15/15, (b) composite 80/10/10, and (c) composite 90/05/05 when immersed in SBF solution after 7 days and B) FT-IR spectrum of (a) composite 70/15/15, (b) composite 80/10/10, and (c) composite 90/05/05 when immersed in SBF solution after 14 days.

In vitro Evaluation of Cytotoxicity

For cell transplantation in the tissue engineering, the scaffolds should be biocompatible and nontoxic to the bone cells. So, the scaffold materials were examined by subjecting the cytotoxic to mouse preosteoblast cells. The proliferation of MC3T3-E1 cells in contact with the extraction of the scaffolds was investigated after 7 days of the culture period by using of the MTT assay (Figure 9). The addition of SF (with the decrease in the CT content) increased the cell proliferation of the CT/SF/MCM-41 composite scaffolds. There were differences between days 1, 3 and 7 for all groups. As a positive control, the cell incubated with Triton X-100 illustrated a major loss of cell viability. The results revealed an evident increase in cell numbers over time. It was shown that the CT/SF/MCM-41 composite scaffolds were cytocompatible, recommending that these scaffolds were non-toxic to osteoplastic cells.

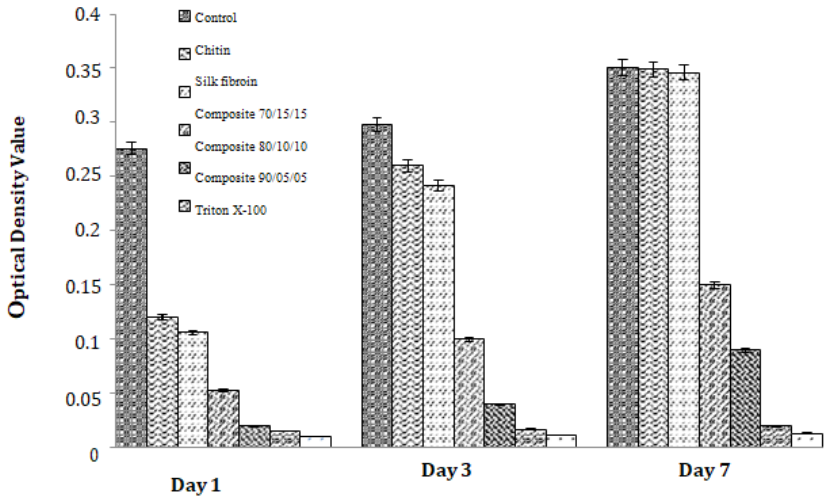

Figure 9: In vitro cytotoxicity evaluation of MC3T3-E1 cells in contact with scaffolds for different periods of time. Data are presented as the mean ± SD (n=5). Significant difference ($p \leq 0.05$).

Cell Attachment Studies

Figure 10 represents the typical SEM of the composites after 7 days of incubation in the cell culture medium following incubation with cells. The attachment and spreading nature of cells on the composite scaffolds were evaluated using this technique. The higher attachment on the composite 70/15/15 scaffold could be due to the increase in surface area because of the presence of MCM-41 in the scaffolds. An increase in the surface area allowed the maximum area for cell attachment, and nano surfaces had a larger surface area to volume ratio. The results indicated that the CT/SF/MCM-41 nanocomposite scaffolds might be suitable for bone tissue engineering applications.

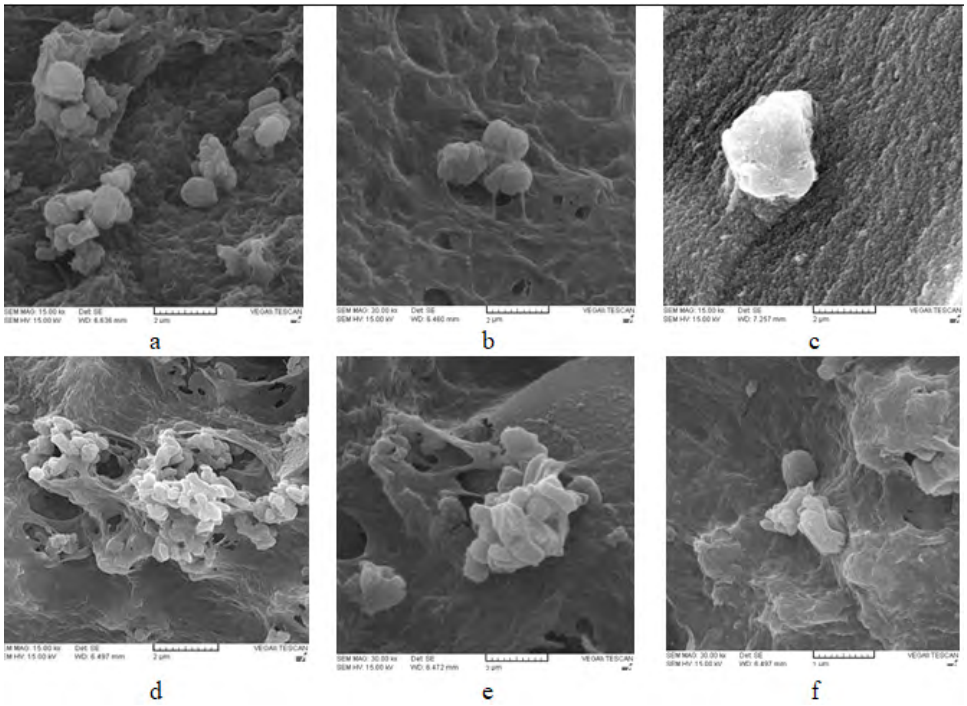

Figure 10: SEM images of (a) composite 70/15/15, (b) composite 80/10/10, and (c) composite 90/05/05 when immersed in culture medium after 3 days. SEM images of (d) composite 70/15/15, (e) composite 80/10/10, and (f) composite 90/05/05 when immersed in culture medium after 7 days.

Conclusion

CT/SF/MCM-41 composite scaffolds were synthesized by using the freeze-drying approach. The resulted scaffolds were characterized and compared together. The composite scaffolds were found to have the favorable pore size and porosity. The mechanical and biological characteristics of the scaffolds were influenced by the addition of the MCM-41 content and changing the ratio of CT and SF in the scaffold. The mechanical and biological properties of the scaffolds were significantly affected by the addition of MCM-41. When MCM-41 was added to CT and SF, density was increased and biodegradability was decreased with a small change in pore size. The increase in density was related to a decrease in the water-uptake capacity and a decrease in the total porosity. MCM-41 substantially improved cell attachment on the scaffold surfaces. Thus, MCM-41 played the role of improving the biological and mechanical properties of the scaffolds at the same time. The addition of MCM-41 to CT and SF provided a more promising scaffold for bone tissue engineering applications.

Acknowledgements

The authors are grateful to the Payame Noor University in Isfahan Research council (Grant # 84910). The authors would like to thank Dr. L. Ghorbanian for the critical reading of the manuscript, and Dr. H. Jalali for technical editing, language editing, and proofreading.

References

1. Nazarov R, Jin HJ, Kaplan DL (2004) Porous 3-D Scaffolds from Regenerated Silk Fibroin. Biomacromol 5(3): 718-726.

2. Wen G, Wang J, Li M, Meng X (2007) Study on tissue engineering scaffolds of silk fibroin- chitosan/nano-hydroxy apatite composite. Key Eng Mater 330: 971-975.

3. Venkatesan J, Qian ZJ, Ryu B, Kumar NA, Kim SK (2011) Preparation and characterization of carbon nanotube-grafted-chitosa-Natural hydroxyapatite composite for bone tissue engineering. Carbohydr Polym 83(2): 569-577.

4. Wang L, Li C (2007) Preparation and physicochemical properties of a novel hydroxyapatite/chitosan silk fibroin composite. Carbohydr Polym 68(4): 740-745.

5. Wu S, Liu X, Yeung KWK, Liu C, Yang X (2014) Biomimetic porous scaffolds for bone tissue engineering. Mater Sci Eng R 80: 1-36.

6. Bhardwaj N, Kundu SC (2011) Silk fibroin protein and chitosan polyelectrolyte complex porous scaffolds for tissue engineering applications. Carbohydr Polym 85(2): 325-333.

7. Gil ES, Frankowski DJ, Hudson SM, Spontak RJ (2007) Silk fibroin membranes from solvent- crystallized silk fibroin/gelatin blends: Effects of blend and solvent composition. Mater Sci Eng C 27(3): 426-431.

8. She Z, Zhang B, Jin C, Feng Q, Xu Y (2008) Preparation and in vitro degradation of porous three- dimensional silk fibroin/chitosan scaffold. Polym Degrad Stab 93(7): 1316-1322.

9. Veparia C, Kaplan DL (2007) Silk as a biomaterial. Prog Polym Sci 32(8-9): 991-1007.

10. Meyers MA, Chen PY, Lin AYM, Seki Y (2008) Biological materials: Structure and mechanical properties. Prog Mater Sci 53(1): 1-206.

11. Jayakumar R, Ramachandran R, Kumar PTS, Divyarani VV, Srinivasan S, et al. (2011) Fabrication of chitin-chitosan/nano ZrO2 composite scaffolds for tissue engineering applications. Int J Biol Macromol 48(2): 336-344.

12. Kumar PTS, Abhilash S, Manzoor K, Nair SV, Tamura H, et al. (2010) Preparation and characterization of novel β-chitin/nanosilver composite scaffolds for wound dressing applications. Carbohydr Polym 80(3): 761-767.

13. Kumar PTS, Srinivasan S, Lakshmanan VK, Tamura H, Nair SV, et al. (2011) β-Chitin hydrogel/nano hydroxyapatite composite scaffolds for tissue engineering applications. Carbohydr Polym 85(3): 584-591.

14. Kumar PTS, Srinivasan S, Lakshmanan VK, Tamura H, Nair SV, et al. (2011) Synthesis, characterization and cytocompatibility studies of α-chitin hydrogel/nano hydroxyapatite composite scaffolds. Int J Biol Macromol 49(1): 20-31.

15. Teymouri M, Samadi-Maybodi A, Vahid A (2011) A rapid method for the synthesis of highly ordered MCM-41. Int Nano Lett 1(1): 34-37.

16. Torney F, Trewyn BG, Lin VS, Wang K (2007) Mesoporous silica nanoparticles deliver DNA and chemicals into plants. Nature Nanotech 2(5): 295-300.

17. Yoshikazu M, Masanori Y, Eiichi A, Sadao A, Shunsuke T (2009) Preparation and adsorption properties of thiol-functionalized mesoporous silica microspheres. Ind Eng Chem Res 48: 938-943.

18. Slowing II, Vivero-Escoto JL, Wu CW, Lin VSY (2008) Mesoporous silica nanoparticles as controlled release drug delivery and gene transfection carriers. Adv Drug

Deliv Rev 60(11): 1278-1288.

19. Kwon S, Singh RK, Perez RA, Abou Neel EA, Kim HW, et al. (2013) Silica-based mesoporous nanoparticles for controlled drug delivery. J Tissue En 4: 1-18.

20. Mortera R, Onida B, Fiorilli S, Cauda V, Vitale Brovarone C, et al. (2008) Synthesis and characterization of MCM-41 spheres inside bioactive glass-ceramic scaffold. Chem Eng J 137(1): 54-61.

21. Izquierdo-Barba I, Colilla M, Vallet-Regi M (2008) Nanostructured mesoporous silicas for Bone Tissue regeneration. J Nanomater pp: 1-14.

22. Mortera R, Baino F, Croce G, Fiorilli S, Vitale-Brovarone C, et al. (2010) Monodisperse Mesoporous Silica Spheres Inside a Bioactive Macroporous Glass-Ceramic Scaffold. Adv Eng Mater 12(7): 256-259.

23. Heikkila T, Salonen J, Tuura J, Kumar N, Salmi T, et al. (2007) Evaluation of mesoporous TCPSi, MCM-41, SBA-15, and TUD-1 materials as API carriers for oral drug delivery. Drug Deliv 14(6): 337-347.

24. Lopez-Noriega A, Arcos D, Izquierdo-Barba I, Sakamoto Y, Terasaki O, et al. (2006) Ordered mesoporous bioactive glasses for bone tissue regeneration. Chem Mater 18(13): 3137-3144.

25. Yoo CR, Yeo IS, Park KE, Park JH, Lee SJ, et al. (2008) Effect of chitin/silk fibroin nanofibrous bicomponent structures on interaction with human epidermal keratinocytes. Int J Biol Macromol 42(4): 324-334.

26. Falini G, Weiner S, Addadi L (2003) Chitin-silk fibroin interactions: relevance to calcium carbonate formation in invertebrates. Calcif Tissue Int 72: 548-554.

27. Jin J, Hassanzadeh P, Perotto G, Sun W, Brenckle MA, et al. (2013) A biomimetic composite from solution self-assembly of chitin nanofibers in a silk fibroin matrix. Adv Mater 27(32): 4482-4487.

28. Park KE, Jung SY, Lee SJ, Min BM, Park WH (2006) Biomimetic nanofibrous scaffolds: preparation and characterization of chitin/silk fibroin blend nanofibers. Int J Biol Macromol 38(3-5): 165-173.

29. Anunziata OA, Martinez ML, Beltramone AR (2009) Hydroxyapatite/MCM-41 and SBA-15 nano- composites: preparation, characterization and applications. Mater 2(4): 1508-1519.

30. Teimouri A, Ghorbanian L, Najafi Chermahini A, Emadi R (2014) Fabrication and characterization of silk/forsterite composites for tissue engineering applications. Ceram Int 40(5): 6405-6411.

31. Ghorbanian L, Emadi R, Razavi SM, Shin H, Teimouri A (2013) Fabrication and characterization of novel diopside/silk fibroin nanocomposite scaffolds for potential application in maxillofacialbone regeneration. Int J Biol Macromol 58: 275-280.

32. Teimouri A, Ebrahimi R, Emadi R, Hashemi Beni B, Najafi Chermahini A (2015) Nano-composite of silk fibroin-chitosan/Nano ZrO2 for tissue engineering applications: fabrication and morphology. Int J Biol Macromol 76: 292-302.

33. Teimouri A, Ebrahimi R, Najafi Chermahini A, Emadi R (2015) Fabrication and characterization of silk fibroin/chitosan/Nano γ-alumina composite scaffolds for tissue engineering applications. RSC Adv 5: 27558-27570.

34. Teimouri A, Azadi M, Emadi R, Lari J, Najafi Chermahini A (2015) Preparation, characterization, degradation and biocompatibility of different silk fibroin based composite scaffolds prepared by freeze-drying method for tissue engineering application. Polym Degrad Stab 121: 18-29.

35. Azadi M, Teimouri A, Mehranzadeh G (2016) Preparation, characterization and biocompatible properties of β-chitin/silk fibroin/nanohydroxyapatite composite scaffolds prepared by freeze- drying method. RSC Adv 6: 7048-7060.

36. Teimouri A, Azadi M, Shams Ghahfarokhi Z, Razavizadeh R (2016) Preparation and characterization of novel β-chitin/ nanodiopside/ nanohydroxyapatite composite scaffolds for tissue engineering applications. J Biomater Sci Polym Ed 28(1): 1-14.

37. Teimouri A, Azadi M (2016) β-Chitin/gelatin/nanohydroxyapatite composite scaffold prepared through freeze-drying method for tissue engineering applications. Polym Bull 73: 3513-3529.

38. Teimouri A, Azadi M (2016) Preparation and characterization of novel chitosan/ nanodiopside/nanohydroxyapatite composite scaffolds for tissue engineering applications. Int J Polymer Mater Polymer Biomater 65: 917-927.

39. Tamura H, Nagahama H, Tokura S (2006) Preparation of chitin hydrogel under mild conditions. Cellulose 13: 357-364.

40. Bhardwaj N, Chakraborty S, Kundu SC (2011) Freeze-gelled silk fibroin protein scaffolds for potential applications in soft tissue engineering. Int J Biolog Macromol 49(3): 260-267.

41. Kokubo T, Takadama H (2006) How useful is SBF in predicting in vivo bone bioactivity?. Biomaterials 27(15): 2907-2915.

42. Li J, Dou Y, Yang J, Yin Y, Zhang H, et al. (2009) Surface characterization and biocompatibility of micro- and nano-hydroxyapatite/chitosan-gelatin network films. Mater Sci Eng C 29(4): 1207-1215.

43. Marque AP, Reis RL (2005) Hydroxyapatite reinforcement of different starch-based polymers affects osteoblast-like cells adhesion/spreading and proliferation. Mater Sci Eng 25(2): 215-229.